Diffraction from planar faults in the halite structure

1990 J. Phys.: Condens. Matter 2 7725

(http://iopscience.iop.org/0953-8984/2/38/001)

J. Phys.: Condens. Matter **2** (1990) 7725–7732. Printed in the UK

Diffraction from planar faults in the halite structure

F W Arnoth†, Maurice Wade‡ and G P Mohanty§

† Dupont Engineering Development Laboratory, Wilmington, DE 19898, USA

‡ Morris Brown College, Atlanta, GA 30314, USA

§ University of North Carolina, Charlotte, NC 28223, USA

Received 8 May 1990

Abstract. Diffraction effects due to planar faults in the halite (B1-type) structure consistent with its slip mode and geometry have been considered. The main effect on the powder pattern is found to be symmetric peak broadening which varies from one reflection to another and leads to an anisotropic particle size effect characteristic of the fault type. The results are compared with the broadening data for two B1 compounds, PbSe and PbTe, both of which show appreciable particle size anisotropy in the cold worked state. It is shown that the observed anisotropy can be satisfactorily rationalised in terms of $a/4[001](110)$-type faults. Quantitative estimations of fault density and other substructural parameters have been given.

1. Introduction

Possibility of dislocation reactions and faulting in the halite (B1-type) structures has been considered by several authors. Raching [1], based on bonding and the observed [001](110) slip system in PbTe suggested the possibility of symmetric splitting of $a[001]$-type dislocations on (110) leading to $(a/2)[001](110)$-type planar faults. This fault, however, places like atoms in close proximity and unless the ordering energy is negligible, a further dissociation given by

$$(a/2)[001] \rightarrow (a/4)[001] + (a/4)[001]$$

may occur with an associated fault of the type $(a/4)[001](110)$. In more ionic crystals, where [110] slip is favoured over [001], Fontaine [2] has considered the analogous dissociation of $(a/2)[110]$ full dislocations on $(\bar{1}10)$ and has given a calculation of the energy of the resulting $(a/4)[110](\bar{1}10)$-type faults for a number of alkali halides. On the experimental side, pressure dependence of flow stress and creep behaviour of several alkali halides have been interpreted in terms of split dislocations and faulting on (110) and an estimation of fault energy from experimental creep data has been given, in reasonable agreement with Fontaine's calculations [3, 4]. Further, electron microscopy observations on PbTe have given evidence of dislocation arrays and pairing and streaking in diffraction patterns, although the origins of some of these features have not been fully established [5, 6]. Morawiec and Mizera [6], however, identified dislocations in PbTe thin films as being of $(a/2)[011]$ type operative on (100) in contrast with the $a[001]$ dislocations considered by Rachinger [1] based on observations of cubic slip in prismatic punching experiments on bulk single crystals. Apparently different slip modes may be

0953-8984/90/387725 + 08 $03.50

operative in this material depending upon deformation condition and possibly temperature to some extent [1, 7, 8].

It is known that faulting can lead to diffraction line broadening characteristic of an anisotropic particle size effect in the material with the broadening, in general, dependant on the diffraction plane and crystal direction [*hkl*]. There have been reports of such particle size anisotropy in cold worked and vapour deposited PbTe without however a full accounting of the source of this behaviour [9, 10]. In this communication we present results indicating similar behaviour for the isomorphous phase PbSe following deformation at room temperature. A new set of measurements on PbTe is also included for comparison. Diffraction effects due to various fault types in the B1 structure are considered and an analysis of the observed anisotropy based on contributions to broadening from planar faults in the cold worked material is presented.

2. Experimental procedure

Stoichiometric samples of PbSe and PbTe were prepared by melting pressed powder compacts of high purity constituent elements in quartz capsules under argon. For the cold worked substructure studies deformation was introduced by grinding the solid samples in a ball mill to −325 size at room temperature. Powder peak shapes were determined with crystal monochromated Cu Kα radiation for two orders of reflection along each of the directions, [100], [110], [111] and [311]. The measured peak profiles were corrected for instrumental broadening by the Stokes method [11] which yielded for each reflection a set of cosine Fourier coefficients, $A(L)$, where L is a length normal to the reflecting plane (hkl). The sine coefficients representing the asymmetric components of the peak profiles were small enough to be negligible.

3. Results and analysis

The cosine coefficients permit an analysis of the symmetric peak broadening in terms of the two dominant substructural features in the cold worked material, that is, non-homogeneous strain, represented by the quantity root mean squared strain (RMSS),

Table 1. Particle size results for PbSe and PbTe.

Reflection pair	D_c (nm)			
	PbSe	PbTe		
	a	a	b	c
(111)/(222)	78	86	86	91
(200)/(400)	112	99	88	278
(220)/(440)	39	47	42	—
(311)/(622)	52	67	—	—

[a] This work.
[b] [9] (cold worked sample).
[c] [10] (vapour deposited thin film data using single-reflection variance method).

$\langle \varepsilon_{hkl}^2 \rangle^{1/2}$, and a generalised small particle size effect represented by the effective particle size parameter, $D_{e,hkl}$, which includes small coherent domain size and possible planar faults contributions [12]. $D_{e,hkl}$ values were deduced through an analysis of the coefficients $A(L)$ by the Warren–Averbach multiple-order method [12] using the reflection pairs (111)/(222), (200)/(400), (220)/(440) and (311)/(622), respectively, and are listed in table 1. The table also lists for comparison earlier particle size results for cold worked and vapour deposited PbTe taken from the literature [9, 10]. A characteristic feature of the results for both compounds is that the particle size along [100] is the largest, the [110] particle size is the smallest with the [111] and [311] falling in between. The observed anisotropy is rather large and is of such a nature that it can not be satisfactorily explained by simple preferentially oriented incoherent internal boundaries [9, 13]. We consider therefore possible contributions from stacking disorder which can also produce [*hkl*] dependence of the particle sizes. For this purpose the analytical form of the multiple order particle size is first written in terms of its two contributing factors [14]:

$$1/D_{e,hkl} = 1/D + 1/D_f^* \tag{1}$$

where

$$1/D_f^* = t^{-1}(h_2^2/D_{f1} - h_1^2/D_{f2}). \tag{2}$$

Here D_{f1} and D_{f2} refer to the fictitious particle sizes due to faulting for the two orders $(h_1k_1l_1)$ and $(h_2k_2l_2)$ used in the multiple-order analysis, $t = (h_2^2 + k_2^2 + l_2^2) - (h_1^2 + k_1^2 + l_1^2)$, and D is a measure of the average coherent domain size in the crystal which is assumed to be isotropic. For the three fault types discussed in section 1, $1/D_f$ values representing symmetric powder peak broadening were calculated using the Warren–Merring method [15, 16], with the assumption that all faults are single-layer intrinsic-type and occur randomly on a set of slip planes within the coherent domain with a density $\alpha \ll 1$. The $1/D_f$ values for the individual reflections and the $1/D_f^*$ values (calculated using (2)) for different multiple-order pairs are listed in tables 2 and 3, respectively, in the units of α/a. (Results for a fourth fault type, also listed in these tables, are discussed later.) None of the faults considered predict peak shift or asymmetry in the powder pattern. It is seen that the $1/D_f$ values for the three faults types vary from one reflection to another as well as among different orders of the same reflection. Since this leads to different patterns of anisotropy in D_f^* and hence D_e values for different faults (equation (1)), importance of various faulting models may be tested by comparing the measured

Table 2. $(1/D_f)$ parameter for planar faults in the B1 structure†.

	{*hkl*}								
Fault type	111	200	220	311	222	400	440	622	444
$(a/2)[001](110)$[a]	2.31	0	0	2.81	0	0	0	0	0
$(a/4)[110](\bar{1}10)$[b]	0	2.66	1.88	1.60	0	0	0	0	0
$(a/4)[001](110)$	1.15	0	1.88	1.40	2.31	0	0	2.80	0
$(a/4)[011](100)$	1.15	0	1.88	1.00	0	0	0	0	0

† In units of α/a, where α is the respective fault density and a is the lattice parameter.

[a] [1].

[b] [2].

Table 3. Multiple-order $1/D_f^*$ parameter (equation (2)) for different fault types†.

	Reflection pair			
Fault type	(111)/(222)	(200)/(400)	(220)/(440)	(311)/(622)
$(a/2)[001](110)$	3.08	0	0	3.76
$(a/4)[110](\bar{1}10)$	0	3.55	2.51	2.14
$(a/4)[001](110)$	0.77	0	2.51	0.94
$(a/4)[110](001)$	1.54	0	2.51	1.34

† In units of α/a, where α is the respective fault density and a is the lattice parameter.

particle size ratios with the D_f^* ratios (table 4). An examination of the results in table 4 shows that on this basis we may rule out the $(a/2)[001](110)$ or the Rachinger model [1] as it predicts no broadening for reflections along [110] for which the smallest particle size has been consistently observed. Similarly the Fontaine model [2], $(a/4)[110](\bar{1}10)$ type, may be ruled out since it broadens (200) the most and predicts the smallest particle size along [100] for which the largest D_e is observed. In fact a close examination indicates that the $(a/4)[001](110)$ fault shows the most satisfactory matching between the D_f^* and the experimental D_e ratios for both PbSe and PbTe.

A similar conclusion is also reached by a different method of analysis which employs the cosine coefficients of individual reflections rather than pairs and is based on the assumption that $\langle \varepsilon_{hkl}^2 \rangle^{1/2}$ is inversely proportional to the Young's modulus along $[hkl]$; that is, $\langle \varepsilon_{hkl}^2 \rangle^{1/2} = k' C_{hkl}$, where C_{hkl} is the reciprocal of the $[hkl]$ modulus and k' is a constant [17]. The quantity C_{hkl} may be computed from the elastic constants of the material [18]. With this assumption the cosine coefficients may be written as

$$-\ln A_{hkl} = L/D + L/D_{f,hkl} + k(C_{hkl}h_i)^2 \tag{3}$$

where $k = 2k'\pi^2 L^2/a^2$. According to (3) a plot of $\ln A_{hkl}$ versus $(C_{hkl}h_i)^2$ should be free from any scatter due to strain broadening and yield a straight line for all (hkl) irrespective of strain anisotropy. Any deviation from linearity of such a plot will be from contributions other than strain, in particular due to the (hkl) dependence of the fault term, L/D_f. Thus by comparing the pattern of distribution of points in a plot of the measured $\ln A_{hkl}$ versus

Table 4. Comparison of the measured particle size ratios for PbSe and PbTe with the predicted D_f^* ratios.

	Reflection pairs			
Fault type	(111)/(222)	(200)/(400)	(220)/(440)	(311)/(622)
$(a/2)[001](110)$	1.22	∞	∞	1.00
$(a/4)[110](\bar{1}10)$	∞	0.71	1.00	1.17
$(a/4)[001](110)$	3.26	∞	1.00	2.67
$(a/4)[110](001)$	1.62	∞	1.00	1.87
Experimental				
PbSe	2.00	2.87	1.00	1.34
PbTe	1.83	2.11	1.00	1.43

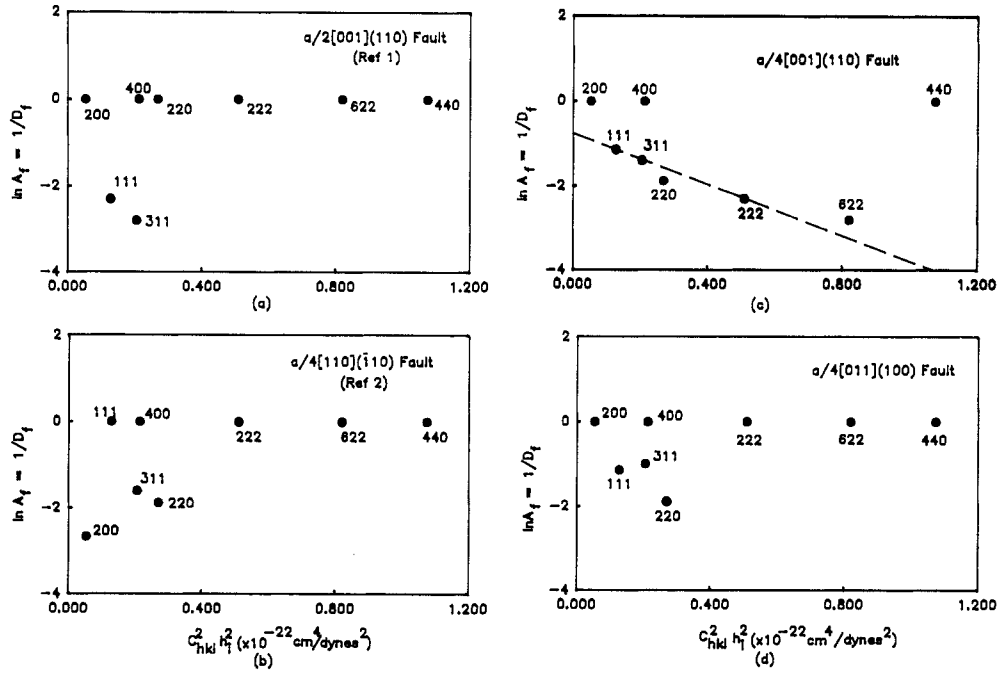

Figure 1. The logarithm of the fault coefficient, $\ln A_f = -(1/D_f)$, in units of $L\alpha/a$, versus $(C_{hkl}h_i)^2$. The full circles represent calculated $1/D_f$ values for different planar faults in the halite structure (fault types identified in the figure insets). C_{hkl} is the reciprocal $[hkl]$ Young's modulus calculated using the elastic constant data for PbTe and $h_i^2 = h^2 + k^2 + l^2$.

$(C_{hkl}h_i)^2$ for fixed L with the corresponding theoretical plots based on the calculated $1/D_f$ parameters, it should be possible to distinguish between the importance of different fault types in a given case [17]. In figures 1(*a*)–1(c) the plots for the three fault types discussed above and in figures 2(*a*) and 2(*b*) the experimental plots for PbSe and PbTe for $L = 12$ nm are given. C_{hkl} values for these plots were calculated using the elastic constant data for PbTe [19]. It is evident from these figures that the Rachinger [1] and the Fontaine [2] models cannot reproduce the experimental pattern of points and thus

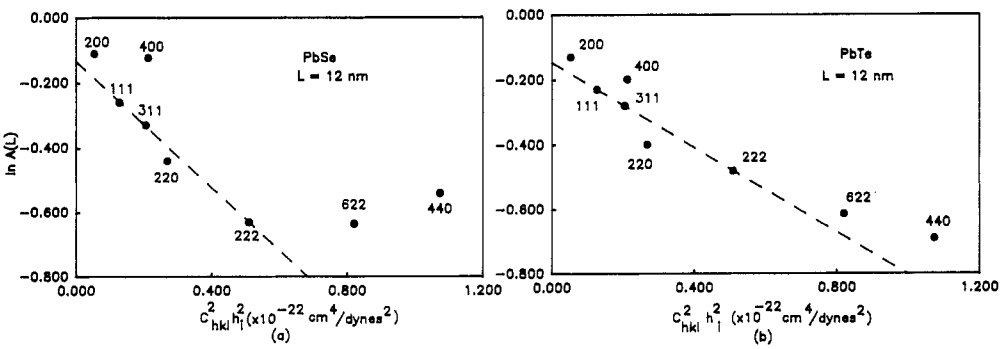

Figure 2. Logarithm of the experimental Fourier coefficient, $\ln A(L)$ versus $(C_{hkl}h_i)^2$ for (*a*) PbSe and (*b*) PbTe; $L = 12$ nm.

Table 5. Least squares solutions for fault density α, domain, size D (nm), strain parameter k' (units: 10^{17} dyne^2 cm^{-4}), coefficient of determination r^2 and standard error estimates.

	PbSe		PbTe	
	a	b	a	b
α	0.0041 ± 0.0001	0.0054 ± 0.0010	0.0029 ± 0.0005	0.0023 ± 0.00072
D	103 ± 23	159 ± 79	104 ± 11	103 ± 22
k'	—	5.73 ± 0.45	—	7.46 ± 0.60
r^2	0.90	0.96	0.95	0.95

[a] Solutions based on (1) and measured $D_{e,hkl}$ values.
[b] Solutions based on (3) and $A(L)$ values for L = 12 nm.

may be ruled out. In fact a detailed comparison shows that the most satisfactory match between the observed and the predicted distributions occurs for the $(a/4)[001](110)$ fault. Specifically it is worth noting that for this model the (111), (311) and (222) points lie on a straight line with a negative slope with the (220) point slightly below and the remaining points above this line. Among the two compounds the scatter of points for PbSe is more pronounced. It also matches more closely the predicted distribution.

Based on the above considerations, assuming that the observed particle size anisotropy is entirely due to the $(a/4)[001](110)$ fault, one may solve for the fault density α and isotropic particle size D using (1) and the experimental D_e values. A least squares fit yielded the solutions given in table 5 which also lists standard error estimates and the coefficient of determination (r^2) deduced from the analysis. Alternatively we may use (3) and the measured coefficients $A(L)$ for fixed L and solve for the parameters k, α, and D. The results of a regression analysis utilising the $A(L)$ for L = 12 nm are given in table 5. The nature of the fit is shown by the listed r^2 values and also through a comparison of the back calculated $A(L)$ (using the least square solutions) with the corresponding experimental $A(L)$ for two values of L in figure 3.

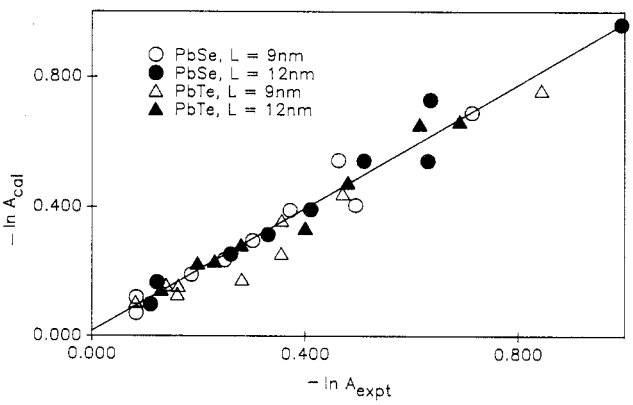

Figure 3. Logarithm of the experimental Fourier coefficient, $\ln A(L)_{exp}$, for PbSe and PbTe, versus $\ln A(L)_{cal}$, back-calculated with the least squares solutions for the substructural parameters; L = 9 and 12 nm.

4. Discussion

The results for PbSe and PbTe have shown that while peak broadening is relatively low for both compounds it is characterised by well defined anisotropy which can be satisfactorily interpreted in terms specific fault and strain contributions. Particle size anisotropy has also been previously reported in vapour deposited PbTe thin films [10]. The source of this anisotropy was not identified; however, it is rather large ($D_{e,100} : D_{e,111} \simeq 3$) and in the same direction as found here for the cold worked materials. As with certain metals and intermetallics showing evidence of particle size anisotropy and faulting [20, 21], in the present case also such behaviour appears to be accompanied by strong anisotropy in the elastic modulus. Using the elastic constant data for PbTe [19], the anisotropy parameter $2C_{44}/(C_{11} - C_{12}) = 2.68/10.03 = 0.26$ at the deformation temperature (300 K). This is an unusually small value for this ratio which indicates possible structural instability with respect to preferentially directed shear and lattice softening in the material.

In conclusion we comment briefly on the $(a/2)[110]$ dislocations reported to be active on (001) in PbTe thin films by Morawiec and Mizera [6]. Assuming symmetric dissociation of such dislocations (in a manner analogous to the Fontaine model [2]) a different type of fault, $(a/4)[011](100)$, would result with a characteristic pattern of broadening. The D_f and D_f^* values for this model are listed in tables 2 and 3 and in figure 1(d) a plot of $\ln A_f$ against $(C_{hkl}h_i)^2$ is given. The D_f^* ratios for this case are seen to be comparable to the $(a/4)[001](110)$ fault (table 4). For example, the ratio of the two limiting particle sizes, that is, the relative [110] and [100] D_e values are correctly predicted by this model (table 4). However, the ratio of the remaining two slightly oversteps the theoretical limit. In particular, the measured $D_{e,311}$ is found to be consistently smaller than $D_{e,111}$ for both compounds opposite to the calculated D_f^* ratio. The discrepancy is more pronounced when one compares the experimental and the predicted $\ln A_f$–$(C_{hkl}h_i)^2$ plots (figures 1(d) and 2). A regression analysis based on (3) and the $1/D_f$ values for this fault yielded solutions for PbSe with unacceptably small r^2 values. Thus, while the possibility of secondary contributions of such faults cannot be ruled out, the diffraction data tend to favour $(a/4)[001](110)$ over this model as the major contributor to the observed broadening.

Acknowledgment

Partial support for this work from the National Science Foundation, Washington, DC, is gratefully acknowledged.

References

[1] Rachinger W A 1956 *Acta Metall.* **4** 647
[2] Fontaine G 1968 *J. Phys. Chem. Solids* **29** 209
[3] Fontaine G and Haasen P 1969 *Phys. Status Solidi* **31** K67
[4] Mohamed F A and Langdon T G 1974 *J. Appl. Phys.* **45** 1965
[5] Levine E and Tauber R N 1968 *J. Electrochem. Soc.* **115** 107
[6] Morawiec J and Mizera E 1981 *Phys. Status Solidi* **63** k1
[7] Buerger M J 1930 *Am. Mineral.* **15** 174
[8] Gilman J J 1959 *Acta Metall.* **7** 608

[9] Mohanty G P and Wert J J 1963 *Trans. Metall. Soc. AIME* **227** 282
[10] Sinha N L P, Samantary B K, Chaudhuri A K and Bose H N 1976 *J. Phys. D: Appl. Phys.* **9** 795
[11] Stokes A R 1948 *Proc. Phys. Soc.* **61** 382
[12] Warren B E 1969 *X-Ray Diffraction* (Reading, MA: Addison-Wesley) p 251
[13] Warren B E 1959 *Prog. Met. Phys.* **8** 147
[14] Mohanty G P and Schmidt R A 1970 *J. Appl. Phys.* **41** 3573
[15] Warren B E and Warekois E P 1953 *J. Appl. Phys.* **24** 951
[16] Wagner C N J, Tetelman A S and Otte H M 1962 *J. Appl. Phys.* **33** 3080
[17] Mohanty G P and Yu T C 1972 *J. Appl. Phys.* **43** 1994
[18] Greenough G B 1952 *Prog. Met. Phys.* **3** 176
[19] Houston B, Strakna R E and Belson H S 1968 *J. Appl. Phys.* **39** 3913
[20] Aqua E N and Wagner C N J 1964, *Phil. Mag.* **9** 56
[21] Mohanty G P and Schmidt R A 1970 *J. Appl. Phys.* **41** 3582